JACS
JOURNAL OF THE AMERICAN CHEMICAL SOCIETY
Article
pubs.acs.org/JACS

Wafer-Scale Transfer of Vertically Aligned Carbon Nanotube Arrays

Miao Wang,[†,‡] Taotao Li,[†] Yagang Yao,*[,†] Huifen Lu,[†] Qiang Li,*[,‡] Minghai Chen,[†] and Qingwen Li[†]

[†]Key Lab of Nanodevices and Applications, Suzhou Institute of Nano-tech and Nano-bionics, Chinese Academy of Sciences, Suzhou 215123, China

[‡]School of Power and Energy Engineering, Nanjing University of Science and Technology, Nanjing 210094, China

Supporting Information

ABSTRACT: The first critical step in making vertically aligned carbon nanotube (VACNT)-based thermal interface materials is to transfer the VACNTs on a large scale. Although VACNTs have been transferred by several methods, they were only transferred inadvertently in most cases. Here we report well-controlled weak-oxidation-assisted transfer of VACNTs. Specifically, after a short time of weak oxidation, we found that VACNTs could be easily detached from the native growth substrates, and thus, a freestanding VACNT film was obtained. Then the VACNTs could be assembled onto specific substrates for its real applications. More importantly, the repeated growth−transfer synthesis of VACNT arrays can be realized in one batch by introducing an additional process of weak oxidation in chemical vapor deposition, which makes the strategy more effective. Surprisingly, no degradation in the quality was observed before and after the weak oxidation according to thermogravimetric analysis and Raman spectra of VACNTs. Enhanced thermal and mechanical properties were achieved after reactive ion etching (RIE) and subsequent metallization of the surfaces of the VACNTs, and this might be due to the removal of impurities such as amorphous carbon and entangled CNTs by RIE. These findings provide an efficient approach for transferring VACNTs, which is important for the application of VACNTs in thermal management.

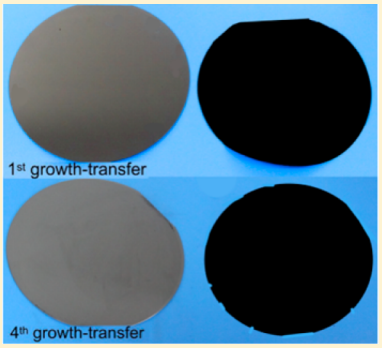

INTRODUCTION

Vertically aligned carbon nanotubes (VACNTs)[1−6] possess superior thermal[7−11] and physical properties[12−15] that make them ideal candidates for use in advanced thermal interface materials (TIMs) to enhance heat dissipation.[16−24] Normally, the VACNT arrays are produced by chemical vapor deposition (CVD), which can grow high-density and high-quality CNTs, but because of the potential incompatibility of the catalyst with the growth substrate and the high growth temperature of VACNTs (above 500 °C), which is not compatible with many semiconductor and packaging assembly processes, the VACNT arrays must be transferred onto specific substrates in order to be assembled on the back side of the chip for thermal management. An advanced transfer technology that is capable of transferring CNTs on a large scale and maintaining well-aligned CNT structures is crucial to realize the applications of VACNTs in electronic packaging. Usually, transfer media such as polymers,[25] solder,[26,27] and thermally conductive adhesives[28] were applied to transfer the VACNT arrays. However, the complicated process may limit their usage. Other transfer techniques, including mechanical detachment, etching-off of the SiO_2 layer, and spontaneous detachment using hot water, have been developed to transfer the VACNT arrays on a larger scale, but the resulting films are easily broken or have to be kept in water to prevent collapse.[29−32]

In this paper, we present well-controlled weak-oxidation-assisted transfer of VACNTs. Briefly, after a short time of weak oxidation, VACNTs can be easily detached from the growth substrates, and thus, a freestanding VACNT film is obtained. With this strategy, the VACNTs can be assembled onto specific substrates for their real applications. More importantly, the repeated growth−transfer synthesis of VACNT arrays can be realized in one batch, which makes the strategy more effective. Surprisingly, no degradation in the quality was observed before and after the weak oxidation according to thermogravimetric analysis (TGA) and Raman spectra of VACNTs. Enhanced thermal and mechanical properties were achieved after reactive ion etching (RIE) and subsequent metallization of the surfaces of the VACNTs, and this might be due to the removal of impurities such as amorphous carbon and entangled CNTs by RIE. These findings provide an efficient approach for transferring VACNTs, which is important for the applications of VACNTs in thermal management.

EXPERIMENTAL SECTION

Growth of VACNT Arrays. The VACNT arrays were synthesized in a 4 in. quartz tube at 750 °C by CVD. The catalyst was prepared by depositing an alumina layer (10 nm) and an iron layer (1 nm) on a silicon substrate with thermal oxide. Argon with 6% hydrogen and pure ethylene were used as the forming gas and the carbon source, respectively. The total flow rate of gases was set at 1.5 L/min. The growth chamber was kept at 750 °C for 5 min until the VACNTs had reached approximately 300 μm in thickness. After cooling to room temperature, the Si wafer deposited with the VACNT array was taken out of the furnance.

Received: November 5, 2014
Published: December 9, 2014

dx.doi.org/10.1021/ja511373g | J. Am. Chem. Soc. 2014, 136, 18156−18162

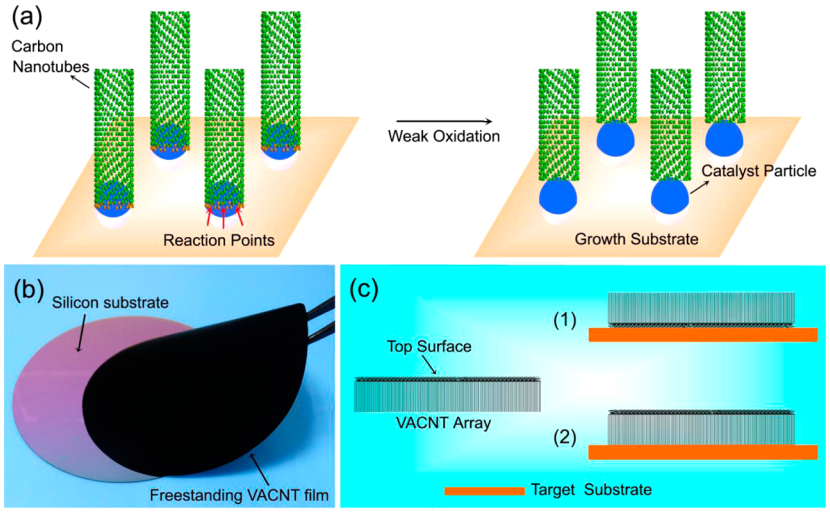

Figure 1. Transfer process of CNT arrays. (a) Schematic diagram of the weak oxidation process. The CNTs at the top of the array are assumed to be close ends. (b) Photograph of a freestanding VACNT film separated from the silicon substrate. (c) Schematic illustration of two types of assembled structures: (1) the top side of the CNT array is bonded to the target substrate; (2) the bottom side of the CNT array is bonded to the target substrate.

Transfer Process. The VACNT arrays were horizontally put into a conventional furnace at different temperatures (300, 400, 450, 490, and 500 °C) for 5 min. Argon was the carrier gas. The oxygen content was below 2% to provide a weak oxidation environment. After the thermal weak oxidation process, the VACNT arrays can be peeled off completely from the silicon substrate as a freestanding film. Additionally, we performed the weak oxidation process during the cooling step of CVD, thus realizing the growth−transfer synthesis of VACNT arrays in one batch. The adhesion agent was uniformly spread onto the target substrate by the spin-coating method. After that, we carefully attached the VACNT films onto the target substrates.

RIE and Metal Deposition. RIE (Tegal 903e) was used to remove the impurities and entangled CNTs on the top surface of VACNT arrays. The oxygen flux, power, and etching time were optimized. At an oxygen flow rate of 7 standard-state cubic centimeters per minute (sccm), a power of 100 W, and an etching time of 2 min, the VACNT arrays showed enhanced crystallinity. After RIE, titanium, nickel, and gold were deposited subsequently on the treated surface of VACNT arrays by electron beam evaporation technology (E-beam 500). The thicknesses of titanium, nickel, and gold were 10, 20, and 300 nm, respectively. Then the RIE and metallization processes were repeated to deposit metals on the other side of the VACNT array. Finally, a sandwich-structure Au−VACNT−Au film was achieved.

Structural Characterization. The VACNT arrays were characterized by scanning electron microscopy (SEM) (FEI Quanta 400 FEG, and HitachiS-4800 HR-FESEM) and high-resolution transmission electron microscopy (HRTEM) (FEI Tecnai G2 F20 S-Twin, 200 kV). The quality of VACNTs was evaluated by Raman spectroscopy (Labram HR 800) and TGA (SDTA851e, PerkinElmer). The Raman measurements were done on the top surface of the VACNT arrays.

Thermal and Mechanical Measurements. The thermal diffusivity of the freestanding VACNT film along the thickness direction was tested by a laser flash thermal analyzer (LFA447, NETZSCH) with a sample size (Φ) of 12.5 mm. The thermal resistance was measured using a DRL-III thermal conductivity meter (Xiangtan City Instrument & Meter Co., Ltd., Xiangtan, China) under a pressure of 40 psi. Mechanical properties were characterized using a nanoindenter (G200, Agilent Technologies). The diameter of the nanoprobe was 250 μm.

RESULTS AND DISCUSSION

Transfer of VACNT Arrays. The basic idea underpinning our transfer approach is outlined in Figure 1a. We grew VACNT arrays on Si wafers using CVD. Electron microscopy images of VACNT arrays are shown in Figure S1 in the Supporting Information. Then the VACNT arrays were exposed to a weak oxidation environment at an optimal temperature, which etched away the active carbon atoms at the root ends of the VACNT arrays with the help of catalyst particles.[33−35] After weakening of the adhesion between the VACNT array and the native growth substrate, the VACNT array was completely detached from the growth substrate. As shown in Figure 1b, a freestanding VACNT array was successfully achieved using our proposed method.

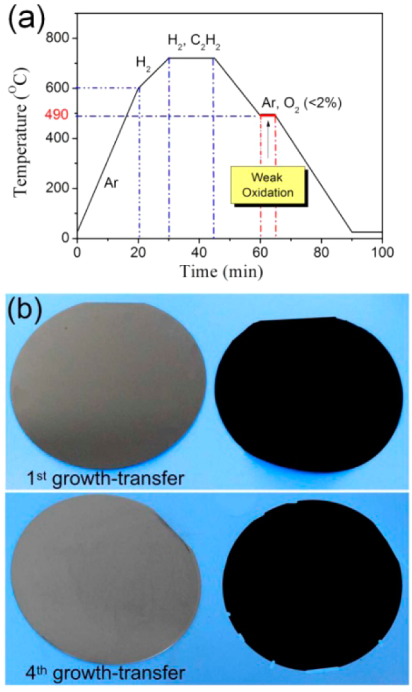

Figure 2. One-batch growth−transfer process. (a) Plot of temperature vs time in CVD for the growth−transfer synthesis of VACNT arrays in one batch. (b) Photograph of two growth−transfer VACNT samples grown using the same $Fe/Al_2O_3/Si$ substrate.

dx.doi.org/10.1021/ja511373g | J. Am. Chem. Soc. 2014, 136, 18156−18162

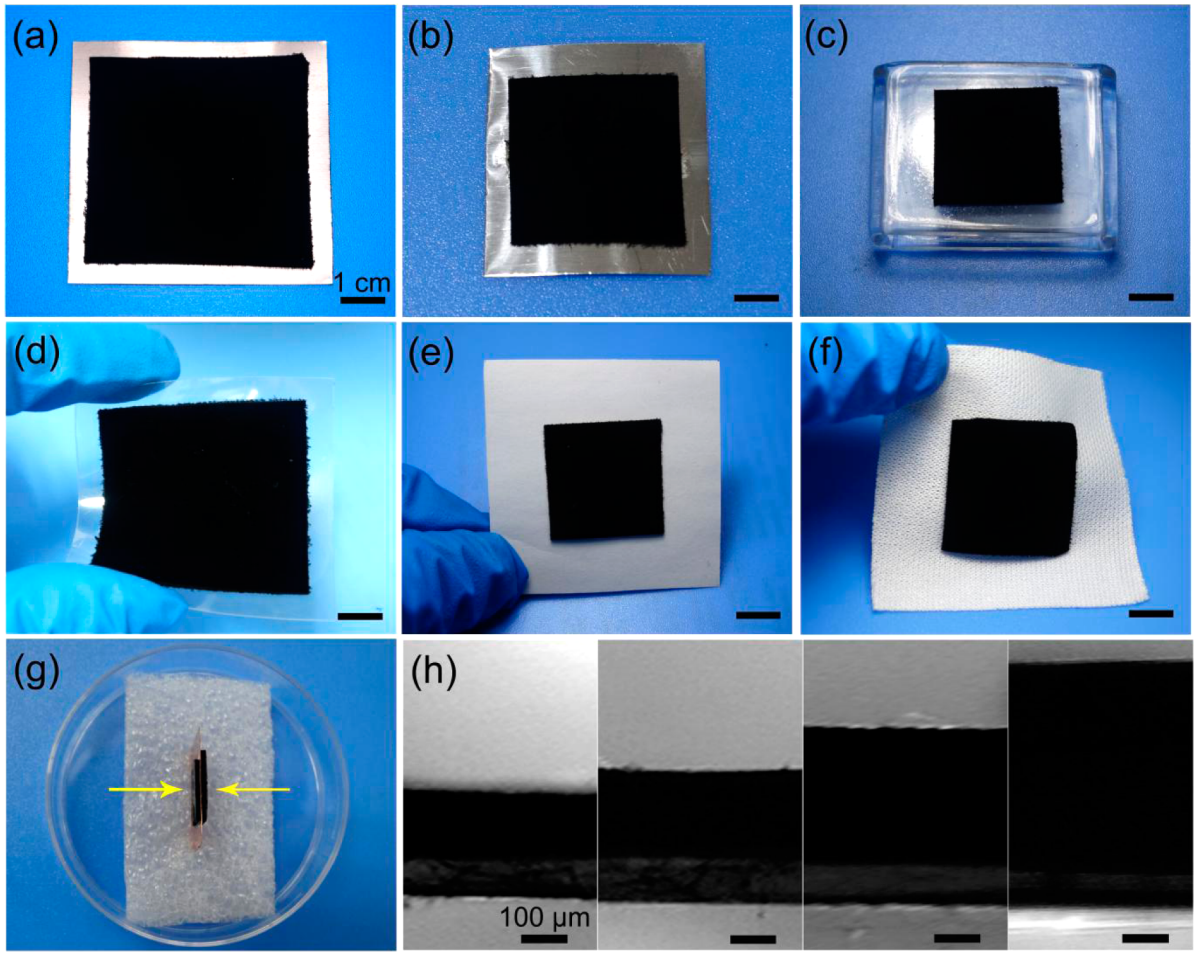

Figure 3. Photographs and optical microscopy images of the transferred samples. (a–f) VACNT arrays were assembled onto target substrates of (a) copper, (b) aluminum, (c) glass, (d) PET, (e) paper, and (f) cloth. (g) Typical photograph of samples transferred onto both sides of a copper foil. (h) Optical microscopy images of transferred VACNT arrays with various heights.

It is well-known that CNTs can be visualized as rolled hexagonal carbon networks that are capped by pentagonal carbon rings. The regions where pentagons are located suffer more strain and thus exhibit higher chemical reactivity compared with regions of purely hexagonal lattices. The root ends of CVD-grown VACNTs, which are wrapped by the catalyst particles, have higher chemical reactivity assisted by the catalytic activity of the metal materials and are the first to be decomposed before the rolled sp^2-hybridized carbon sheets.[30] As shown in Figure 1a, when the proper temperature is reached, the oxygen atoms attack the root ends of the VACNTs, which are the main reaction points. Once the bonding between VACNTs and the growth substrates is weakened, the integrated VACNT arrays can be easily removed from the silicon substrates, affording freestanding VACNT films with areas as large as 4 in., as shown in Figure 1b and Figure S2 in the Supporting Information. It is obvious that this transfer process is simple, convenient, and efficient.

Furthermore, with the above strategy we can easily construct two types of assembled structures, as shown schematically in Figure 1c. One structure, in which the top side of the VACNTs is bonded to the target substrate, can also be obtained by other transfer methods. The other one, in which the bottom side of the VACNTs is assembled onto the target substrate, can only be achieved by our method reported herein. It is well-accepted that the top surface of VACNTs have entangled CNTs and an amount of impurities such as amorphous carbon and catalyst particles, as shown in Figure S3 in the Supporting Information. These result in poor interfacial bonding with the target substrates due to bad wetting of the top surface of VACNTs to the target substrates. The two assembled structures enabled by our transfer method allowed us indirectly to investigate the interface bonding between VACNTs and the target substrates. We assembled VACNTs onto copper foils with thermally conductive adhesives and characterized the total thermal resistance with increasing pressure. The measurement results are shown in Figure S4 in the Supporting Information. Apparently, the samples in which the top side of the VACNTs is bonded to the copper surface have lower thermal resistance and thus stronger interfacial bonding with the target substrates than the samples in which the bottom side is assembled onto the copper.

More importantly, the growth–transfer synthesis of VACNT arrays can be realized in one batch, which saves a lot of energy. As shown in Figure 2a, after the growth of VACNTs at high temperature, an additional weak oxidation process was performed to weaken the adhesion between the VACNT arrays and the growth substrate during the cooling step of CVD. After the sample was removed from the furnace, a freestanding VACNT film with a size of 4 in. was easily obtained, as shown in Figure 2b, demonstrating the successful growth–transfer synthesis of the VACNT arrays in one batch,

dx.doi.org/10.1021/ja511373g | J. Am. Chem. Soc. 2014, 136, 18156–18162

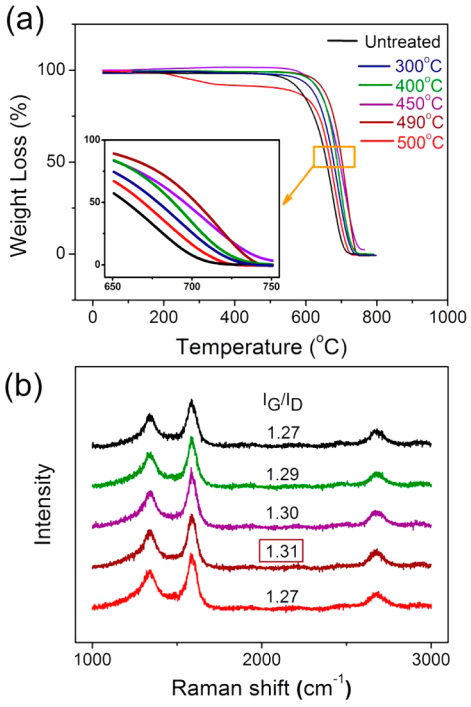

Figure 4. (a) TGA and (b) Raman spectroscopy characterizations of the VACNT arrays before and after the weak oxidation. The VACNT arrays were treated at temperatures of 300 °C (blue line), 400 °C (green line), 450 °C (purple line), 490 °C (dark-red line), and 500 °C (red line) for 5 min. The line colors in (a) and (b) have the same meaning.

which might speed up the applications of VACNTs. In addition, the metal catalysts for the growth of VACNTs can be reused. The catalysts on the silicon surface after the transfer of VACNTs still have features of high activity and freedom from contamination and can be used for secondary growth of VACNT arrays. We repeated the growth−transfer synthesis of VACNT arrays four times with the same $Fe/Al_2O_3/Si$ substrate. The growth conditions for the repeat process were the same as the original growth conditions. Photographs of the transferred VACNTs are shown in Figure 2b. The transferred arrays were well-aligned with high quality, and no obvious bent regions were found (see Figure S5 in the Supporting Information), demonstrating that the silicon substrate and the catalysts can be recycled multiple times for the growth−transfer synthesis of VACNTs. Thus, the repeated growth−transfer synthesis of VACNT arrays in one batch may open up commercial realization of various functional devices based on VACNTs.

Enabled by the proposed method, we were able to assemble VACNT arrays with various heights onto all sorts of substrates with different areas. A series of photographs of the transferred samples are shown in Figure 3. The target substrate can be rigid, such as copper (Figure 3a), aluminum (Figure 3b), or glass (Figure 3c), or flexible, such as poly(ethylene terephthalate) (PET) (Figure 3d), paper (Figure 3e), or cloth (Figure 3f). The transferred VACNT arrays retained their structural integrity and remained undamaged. A typical SEM image of the interfacial micromorphology between the VACNT arrays and the target substrate is shown in Figure S5 in the Supporting Information. It can be seen that the root ends of the VACNT arrays were well-embedded in the adhesion agent, indicating good interfacial bonding. We can also transfer VACNT arrays onto both the top and bottom sides of the copper foil (Figure 3g), which is difficult to realize by prior transfer technology or direct growth of VACNT arrays. Additionally, VACNT arrays with various heights from 100 μm to 2 mm can be transferred (Figure 3h). All of the above results indicate that the proposed method can realize large-area transfer of VACNT arrays onto various kinds of substrates without damage to the well-aligned structure and maintaining the excellent properties of the VACNT arrays, which might address the problems in previous transfer technology.

Because the oxidation process is introduced in the transfer approach, it is necessary to optimize the treatment temperature to ensure high quality of the CNTs after the transfer. An analysis of the quality of the VACNTs was performed using TGA and Raman spectroscopy. The TGA curve of untreated VACNT arrays is shown in Figure 4a. Significant weight loss started to occur at 510 °C, and the weight loss continued to increase rapidly with elevation of the temperature until a stable plateau region appeared at 700 °C. The sample had lost 80% of its mass when the experiment was terminated at 800 °C. This result implies that the treatment temperature for the weak oxidation should be designed under 510 °C in order to avoid etching away of the VACNTs by oxygen. Therefore, we chose treatment temperatures of 300, 400, 450, 490, and 500 °C for 5 min. The oxygen content was below 2% to provide a weak oxidation environment. To evaluate the quality of VACNTs after the transfer, we did TGA and Raman characterizations of VACNTs, and the results are shown in Figure 4. All of the Raman spectra in Figure 4b exhibit a G/D peak intensity ratio around 1.30, which is similar to that before the weak oxidation, indicating that there was no degradation in the quality of the VACNTs after the weak oxidation. As shown by the TGA data in Figure 4a, from 300 to 490 °C, the decomposition temperature of the VACNTs increased as a result of the removal of amorphous carbon in the VACNT arrays. Afterward, the decomposition temperature decreased because the high treatment temperature and oxidation environment may introduce defects in the VACNT arrays, leading to degradation of the VACNTs. As a result, the proper treatment temperature was set at 490 °C to ensure that the VACNT arrays could be completely transferred while maintaining their high quality, which lays a solid basis for the manufacture of TIMs.

Fabrication and Structure of the Au−VACNT−Au Film. The freestanding VACNT films produced by our method allowed us to investigate the thermal and mechanical properties of VACNTs. Usually, VACNT arrays cannot be directly used as TIMs in thermal management because of their mechanical fragility. In order to make the VACNT films mechanically more robust, a thin layer of titanium/nickel/gold was deposited on both the top and bottom surfaces of the freestanding VACNT films.[19,36−38] As mentioned earlier, the top surfaces of pristine VACNT arrays have a layer of amorphous carbon, metal catalyst particle impurities, and entangled CNTs, as shown in Figure 5a and Figure S6a in the Supporting Information, which make the VACNTs rough and difficult for the metal to wet. Thus, it is necessary to remove them before the metallization of the VACNT surfaces. RIE was used to remove the impurities and entangled CNTs on the top surface of the VACNT arrays.[39−43] According to the G/D ratios of the VACNT arrays after RIE (see Table S1 in the Supporting Information), an oxygen flow rate of 7 sccm, an etching time of 2 min, and a power of 100 W for RIE were chosen, and typical SEM images of the surface morphology of the VACNT arrays after RIE are presented in Figure 5b and Figure S6b,c in the Supporting

dx.doi.org/10.1021/ja511373g | J. Am. Chem. Soc. 2014, 136, 18156−18162

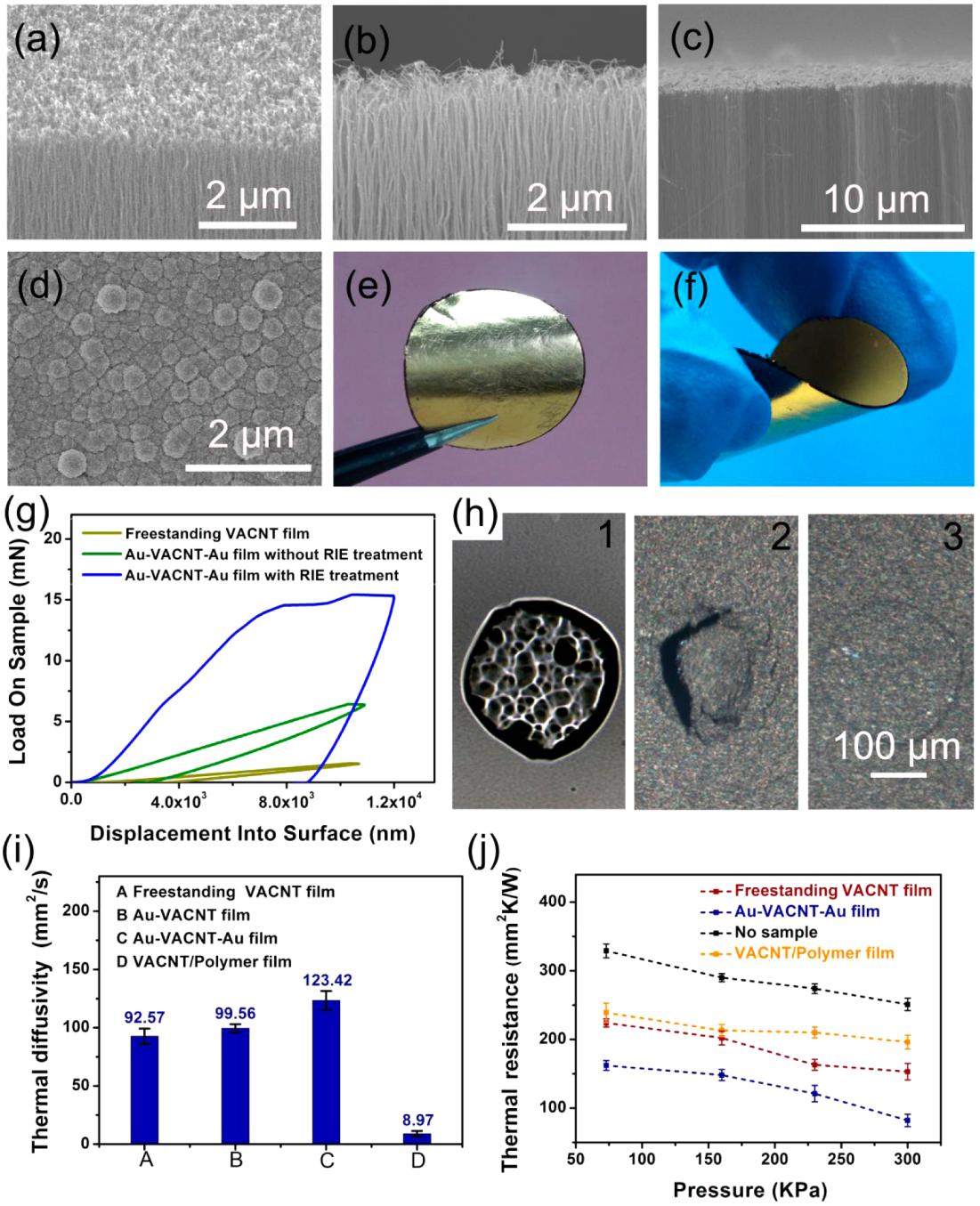

Figure 5. Analysis of freestanding VACNT films. (a–c) Side-view SEM images of (a) the pristine VACNT array, (b) the RIE-treated VACNT array, and (c) the VACNT array coated with a 330 nm-thick metal layer by side view. (d) Top-view SEM image of VACNT array coated with a thin layer of metals. The metal layer was titanium/nickel/gold. (e, f) Photographs of a Au–VACNT–Au film with a thickness of about 300 μm. The sandwich structure has a smooth surface and shows good flexibility without any cracks after bending. (g) Stress–strain curves of Au–VACNT–Au films with and without RIE treatment compared with that of a pristine VACNT array. (h) Optical microscopy images of samples after mechanical tests. (i) Thermal diffusivities and (g) thermal resistances of freestanding VACNT, Au–VACNT, Au–VACNT–Au, and VACNT/polymer films.

Information. It is obvious that most of the impurities and entangled CNTs were removed from the top surfaces because of the oxidation and volatilization of the amorphous carbon and entangled CNTs. Surprisingly, the Raman spectrum (Figure S6d in the Supporting Information) exhibits a higher G/D peak intensity ratio of 2.75 compared with that of the pristine VACNT array (1.31). We believe that in the RIE experiments the oxygen plasma plays a significant role in removing the amorphous carbon covering the outer wall of the VACNTs and the end caps of the CNTs. After RIE, the titanium, nickel, and gold were deposited on the VACNT arrays. The titanium layer provided increased adhesion, and the nickel layer prevented the diffusion of gold. The characterizations of the VACNT arrays coated with titanium/nickel/gold, denoted as Au–VACNT–Au films, are shown in Figure 5c–f and Figure S7 in the Supporting Information. From the cross-section SEM image of the Au–VACNT–Au film in Figure 5c, we can see that the gold was uniformly covered on the surfaces of the VACNT arrays. Especially for the top surface of the VACNT array, as shown in Figure 5d, different sizes of metal particles were

dx.doi.org/10.1021/ja511373g | J. Am. Chem. Soc. 2014, 136, 18156–18162

coated on it, indicating that a flat surface was provided after the RIE process. As shown in Figure 5f, slight bending of the Au−VACNT−Au film with a thickness of 300 μm did not destroy the obtained structure, showing the good flexibility of the sandwiched VACNT films. Also, the CNTs in the middle were still well-aligned and could serve as heat conduction channels between the two layers of gold.

Mechanical and Thermal Properties. The mechanical properties of the obtained VACNT films were characterized using a nanoindenter and the results are shown in Figure 5g. Compared with the VACNTs without RIE treatment and metal deposition, enhanced compression modulus was observed for the sample coated with titanium/nickel/gold on the RIE-treated surfaces, further proving that the RIE process is a good choice for making a flat surface for metal deposition. Figure 5h shows optical microscopy images of the indentations after mechanical tests. When the loaded force was only 7 mN (Figure 5h-1), the original VACNT array was fully collapsed. Upon gold deposition, the VACNT array was much stronger and did not break until the loaded force was above 160 mN (Figure 5h-2), perhaps because the gold coated on the surfaces gathers the loose CNT tips to form a plane that does not easily fall apart. After the metallization on the RIE-treated surfaces, the obtained VACNT film was mechanically the most robust and would not break even under a loaded force of 641 mN (Figure 5h-3), which is close to 2 orders of magnitude higher than that of the original VACNT array. The Au−VACNT−Au film is proved to be a robust and flexible film even when it is bent or compressed.

The thermal properties of the above samples were characterized using a laser flash analyzer (Figure 5i). Similarly, enhanced thermal diffusivity was obtained for the sample that was coated with titanium/nickel/gold on the RIE-treated surfaces. The uniform gold layer covered on the top surface of the VACNT array can serve as a heat current collector, as it is conducive to gathering and transmission of the heat current. Thus, the Au−VACNT−Au film should have a higher thermal diffusivity than the original VACNT array. The thermal resistance was also measured with a thermal conductivity meter to verify the good thermal performance of the sandwiched VACNTs. The sample was put between two copper pillars under a certain pressure. The original VACNT array is believed to be a good TIM to fill the gap between the two copper pillars. However, the poor mechanical properties of the film could result in cracks and thus high thermal resistance. Normally, VACNT arrays are composited with a polymer to improve the mechanical behavior,[34,44−48] but the thermal resistance of such a film was even higher than that of the original VACNT array (Figure 5j), which might be due to the poor interfacial compatibility between the copper pillars and the polymer. By the application of a thin layer of gold on the surfaces of the VACNTs, the effective contact area was greatly increased, so the thermal contact resistance was expected to decrease. As shown in Figure 5j, the thermal contact resistance of the metallized VACNTs was reduced by 50% compared with that of the original VACNTs. The experimental results suggest that metallization is a feasible way to improve the thermal conducting performance of the VACNT arrays.

■ CONCLUSIONS

We have shown a rational approach to transfer VACNT arrays onto arbitrary substrates after a short time of weak oxidation. Moreover, the repeated growth−transfer synthesis of the VACNT arrays can be realized in one batch by introducing an additional process of weak oxidation in CVD. Utilizing this method, we were able to make freestanding VACNT films, which are ideal candidates for use in advanced TIMs to enhance heat dissipation. Enhanced thermal and mechanical properties were achieved by RIE and subsequent metallization of the surfaces of the VACNTs, which is favorable for the applications of VACNTs.

■ ASSOCIATED CONTENT

Ⓢ Supporting Information

Electron microscopy images of VACNT arrays, photograph of a freestanding VACNT film, SEM image of the top surface of VACNT arrays, thermal resistances of two types of assembled structures, cross-section SEM image of transferred VACNT arrays on a target substrate, SEM images and Raman spectra of the representative surfaces of VACNT arrays before and after the RIE process under different treatment conditions, and a photograph of Au−VACNT−Au film released from a silicon substrate. This material is available free of charge via the Internet at http://pubs.acs.org.

■ AUTHOR INFORMATION

Corresponding Authors

ygyao2013@sinano.ac.cn
liqiang@mail.njust.edu.cn

Notes

The authors declare no competing financial interest.

■ ACKNOWLEDGMENTS

This work was supported by the National Natural Science Foundation of China (51225602 and 51372265), the National Basic Research Program (2010CB934700), the Production and Research Collaborative Innovation Project of Jiangsu Province, China (BY2011178), the Natural Science Foundation of Jiangsu Province, China (BK20140392), and the Science and Technology Project of Suzhou, China (ZXG201428 and ZXG201401).

■ REFERENCES

(1) Jiang, K. L.; Li, Q. Q.; Fan, S. S. *Nature* **2002**, *419*, 801.
(2) Zhang, M.; Atkinson, K. R.; Baughman, R. H. *Science* **2004**, *306*, 1358−1361.
(3) Zhang, M.; Fang, S.; Zakhidov, A. A.; Lee, S. B.; Aliev, A. E.; Williams, C. D.; Atkinson, K. R.; Baughman, R. H. *Science* **2005**, *309*, 1215−1219.
(4) Xiao, L.; Chen, Z.; Feng, C.; Liu, L.; Bai, Z. Q.; Wang, Y.; Qian, L.; Zhang, Y. Y.; Li, Q. Q.; Jiang, K. L.; Fan, S. S. *Nano Lett.* **2008**, *8*, 4539−4545.
(5) Zheng, L. X.; O'Connell, M. J.; Doorn, S. K.; Liao, X. Z.; Zhao, Y. H.; Akhadov, E. A.; Hoffbauer, M. A.; Roop, B. J.; Jia, Q. X.; Dye, R. C.; Peterson, D. E.; Huang, S. M.; Liu, J.; Zhu, Y. T. *Nat. Mater.* **2004**, *3*, 673−676.
(6) Yao, Y.; Li, Q.; Zhang, J.; Liu, R.; Jiao, L.; Zhu, Y. T.; Liu, Z. *Nat. Mater.* **2007**, *6*, 283−286.
(7) Li, Q.; Zhang, X.; DePaula, R. F.; Zheng, L.; Zhao, Y.; Stan, L.; Holesinger, T. G.; Arendt, P. N.; Peterson, D. E.; Zhu, Y. T. *Adv. Mater.* **2006**, *18*, 3160−3163.
(8) Shaikh, S.; Li, L.; Lafdi, K. *Carbon* **2007**, *45*, 2608−2613.
(9) Hone, J.; Whiteny, M.; Piskoti, C.; Zettl, A. *Phys. Rev. B* **1999**, *59*, R2514−R2516.
(10) Hone, J.; Llaguno, M. C.; Nemes, N. M.; Johnson, A. T.; Fischer, J. E.; Walters, D. A.; Casavant, M. J.; Schmidt, J.; Smalley, R. E. *Appl. Phys. Lett.* **2006**, *77*, 666−668.

(11) Yang, D. J.; Zhang, Q.; Chen, G.; Yoon, S. F.; Ahn, J.; Wang, S. G.; Zhoui, Q.; Wang, Q.; Li, J. Q. *Phys. Rev. B* **2002**, *66*, No. 165440.
(12) Hu, X. J.; Padilla, A. A.; Xu, J.; Fisher, T. S.; Goodson, K. E. *J. Heat Transfer* **2006**, *128*, 1109−1113.
(13) Zhang, X.; Li, Q.; Tu, Y.; Li, Y.; Coulter, J. Y.; Zheng, L.; Zhao, Y.; Jia, Q.; Peterson, D. E.; Zhu, Y. T. *Small* **2007**, *3*, 244−248.
(14) Zhang, X. B.; Jiang, K. L.; Feng, C.; Liu, P.; Zhang, L. N.; Kong, J.; Zhang, T. H.; Li, Q. Q.; Fan, S. S. *Adv. Mater.* **2006**, *18*, 1505−1510.
(15) Liu, K.; Sun, Y. H.; Lin, X. Y.; Zhou, R. F.; Wang, J. P.; Fan, S. S.; Jiang, K. L. *ACS Nano* **2010**, *4*, 5827−5834.
(16) Zhang, X.; Li, Q.; Holesinger, T. G.; Arendt, P. N.; Huang, J.; Kirven, P. D.; Clapp, T. G.; DePaula, R. F.; Liao, X.; Zhao, Y.; Zheng, L.; Peterson, D.; Zhu, Y. T. *Adv. Mater.* **2007**, *19*, 4198−4201.
(17) Cross, R.; Cola, B. A.; Fisher, T. S.; Xu, X.; Gall, K.; Graham, S. *Nanotechnology* **2010**, *21*, 5705−5713.
(18) Xu, J.; Fisher, T. S. *IEEE Trans. Compon. Packag. Technol.* **2006**, *29*, 261−267.
(19) Panzer, M. A.; Zhang, G.; Mann, D.; Hu, X.; Pop, E.; Dai, H.; Goodson, K. E. J. *J. Heat Transfer* **2008**, *130*, No. 052401.
(20) Maklin, J.; Halonen, N.; Toth, G.; Sapi, A.; Kukovecz, A.; Konya, Z.; Jantunen, H.; Mikkola, J. P.; Kordas, K. *Phys. Status Solidi B* **2011**, *248*, 2508−2511.
(21) Zhang, K.; Chai, Y.; Yuen, M. M. F.; Xiao, D. G. W.; Chan, P. C. H. *Nanotechnology* **2008**, *19*, No. 215706.
(22) Xie, H.; Cai, A.; Wang, X. *Phys. Lett. A* **2007**, *369*, 120−123.
(23) Akoshima, M.; Hata, K.; Futaba, D. N. *Jpn. J. Appl. Phys.* **2009**, *48*, No. 05EC07.
(24) Yang, D.; Zhang, Q.; Chen, G. *Phys. Lett. A* **2002**, *329*, 207−213.
(25) Chen, L.; Zou, R.; Xia, W.; Liu, Z.; Shang, Y.; Zhu, J.; Wang, Y.; Lin, J.; Xia, D.; Cao, A. *ACS Nano* **2012**, *6*, 10884−10892.
(26) Zhu, L. B.; Sun, Y. Y.; Hess, D. W.; Wong, C. P. *Nano Lett.* **2006**, *6*, 243−247.
(27) Kim, M. J.; Nicholas, N.; Kittrell, C.; Haroz, E.; Shan, H.; Wainerdi, T. J.; Lee, S.; Schmidt, H. K.; Smalley, R. E.; Hauge, R. H. *J. Am. Chem. Soc.* **2006**, *128*, 9312−9313.
(28) Chiu, C. C.; Tsai, T. Y.; Tai, N. H. *Nanotechnology* **2006**, *17*, 2840−2844.
(29) Liu, K.; Jiang, K.; Wei, Y.; Ge, S.; Liu, P.; Fan, S. *Adv. Mater.* **2007**, *19*, 975−978.
(30) Huang, J. Q.; Zhang, Q.; Zhao, M. Q.; Wei, F. *Carbon* **2010**, *48*, 1441−1450.
(31) Zhang, G. Y.; Mann, D.; Zhang, L.; Javey, A.; Li, Y. M.; Yenilmez, E.; Wang, Q.; McVittie, J. P.; Nishi, Y.; Gibbons, J.; Dai, H. J. *Proc. Natl. Acad. Sci. U.S.A.* **2005**, *102*, 16141−16145.
(32) Murakami, Y.; Maruyama, S. *Chem. Phys. Lett.* **2006**, *422*, 575.
(33) Hou, P. X.; Liu, C.; Chen, H. M. *Carbon* **2008**, *46*, 2003−2025.
(34) Dementev, N.; Osswald, S.; Gogotsi, Y.; Borquet, E. *J. Mater. Chem.* **2009**, *19*, 7904−7908.
(35) Wang, M.; Chen, H.; Xing, Y.; Wei, H.; Li, Q.; Chen, M.; Li, Q.; Xuan, Y. *J. Nanosci. Nanotechnol.* **2015**, *15*, 3212−3217.
(36) Wu, Y.; Liu, C. H.; Huang, H.; Fan, S. S. *Appl. Phys. Lett.* **2005**, *87*, No. 213108.
(37) Ngo, Q.; Cruden, B. A.; Cassell, A. M.; Sims, G.; Meyyappan, M.; Li, J.; Yang, C. Y. *Nano Lett.* **2004**, *4*, 2403−2407.
(38) Poenitzsch, V. Z.; Slinker, K. A.; Miles, D. W.; Miller, M. A.; Wei, R.; Coulter, K. E.; Gardner, S. H. *J. Mater. Sci.* **2014**, *49*, 7080−7086.
(39) Feng, C.; Liu, K.; Wu, J. S.; Liu, L.; Cheng, J. S.; Zhang, Y. Y.; Sun, Y. H.; Li, Q. Q.; Fan, S. S.; Jiang, K. L. *Adv. Funct. Mater.* **2010**, *20*, 885−891.
(40) Zhi, C. Y.; Bai, X. D.; Wang, E. G. *Appl. Phys. Lett.* **2002**, *81*, 1690−1692.
(41) Chen, Z.; Engelsen, D. D.; Bachmann, P. K.; Elsbergen, V. V.; Koehler, I.; Merikhi, J.; Wiechert, D. U. *Appl. Phys. Lett.* **2005**, *87*, No. 243104.
(42) Burbert, H.; Haiber, S.; Brandl, W.; Marginean, G.; Heintze, M.; Brüser, V. *Diamond Relat. Mater.* **2003**, *12*, 811−815.
(43) Liu, Y.; Liu, L.; Liu, P.; Sheng, L.; Fan, S. S. *Diamond Relat. Mater.* **2004**, *13*, 1609−1613.
(44) Liu, Z.; Zou, R.; Lin, Z.; Gui, X.; Chen, R.; Lin, J.; Shang, Y.; Cao, A. *Nano Lett.* **2013**, *13*, 4028−4035.
(45) Huang, S.; Li, L.; Yang, Z.; Zhang, L.; Saiyin, H.; Chen, T.; Peng, H. *Adv. Mater.* **2011**, *23*, 4707−4710.
(46) Lin, W.; Moon, K. S.; Wong, C. P. *Adv. Mater.* **2009**, *21*, 2421−2424.
(47) Wang, M.; Chen, H.; Lin, W.; Li, Z.; Li, Q.; Chen, M.; Meng, F.; Yao, Y. G.; Wong, C.-p.; Li, Q. *ACS Appl. Mater. Interfaces* **2014**, *6*, 539−544.
(48) Marconnet, A. M.; Yamamoto, N.; Panzer, M. A.; Wardle, B. L.; Goodson, K. E. *ACS Nano* **2011**, *5*, 4818−4825.